Computational Biology and Chemistry 106 (2023) 107934

Contents lists available at ScienceDirect

Computational Biology and Chemistry

journal homepage: www.elsevier.com/locate/cbac

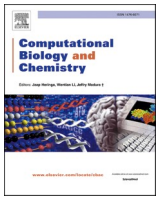

Three candidate anticancer drugs were repositioned by integrative analysis of the transcriptomes of species with different regenerative abilities after injury

Elif Kubat Oktem [a,1,*], Ummuhan Demir [a,b], Metin Yazar [c,d], Kazim Yalcin Arga [d,e]

[a] Department of Molecular Biology and Genetics, Istanbul Medeniyet University, Istanbul, Turkey
[b] Istanbul Medeniyet University, Science and Advanced Technology Research Center (BILTAM), Istanbul, Turkey
[c] Department of Genetics and Bioengineering, Istanbul Okan University, Istanbul, Turkey
[d] Department of Bioengineering, Marmara University, Istanbul, Turkey
[e] Genetic and Metabolic Diseases Research and Investigation Center, Marmara University, Istanbul, Turkey

ARTICLE INFO

Keywords:
Axolotl
Cancer
Bioinformatics
Regenerative medicine
Systems biology
Drug repositioning

ABSTRACT

Regeneration is a homeostatic process that involves the restoration of cells and body parts. Most of the molecular mechanisms and signalling pathways involved in wound healing, such as proliferation, have also been associated with cancer cell growth, suggesting that cancer is an over/unhealed wound. In this study, we examined differentially expressed genes in spinal cord samples from regenerative organisms (axolotl and zebrafish) and non-regenerative organisms (mouse and rat) compared to intact control spinal cord samples using publicly available transcriptomics data and bioinformatics analyses. Based on these gene signatures, we investigated 3 small compounds, namely cucurbitacin I, BMS-754807, and PHA-793887 as potential candidates for the treatment of cancer. The predicted target genes of the repositioned compounds were mainly enriched with the greatest number of genes in cancer pathways. The molecular docking results on the binding affinity between the repositioned compounds and their target genes are also reported. The repositioned 3 small compounds showed anticancer effect both in 2D and 3D cell cultures using the prostate cancer cell line as a model. We propose cucurbitacin I, BMS-754807, and PHA-793887 as potential anticancer drug candidates. Future studies on the mechanisms associated with the revealed gene signatures and anticancer effects of these three small compunds would allow scientists to develop therapeutic approaches to combat cancer. This research contributes to the evaluation of mechanisms and gene signatures that either limit or cause cancer, and to the development of new cancer therapies by establishing a link between regeneration and carcinogenesis.

1. Introduction

Cells and body parts are restored as part of the homeostatic process of regeneration. Most of the molecular mechanisms and signaling pathways involved in wound healing, such as proliferation, have also been linked to cancer cell growth, suggesting the idea that cancer is an over/unhealed wound (Sundaram et al., 2018).

Urodele amphibians (axolotl and newt) and zebrafish, unlike mammals, are among the known regenerating organisms. The axolotl (Ambystoma mexicanum) can regenerate its complex biological structures such as internal organs, spinal cord, brain, tail, and limbs (Demircan, 2020). The ability of axolotl to resist tumor formation and reverse tumorigenesis also attracted the attention of scientists. Regeneration after administration of various carcinogens has also been shown to resist cancer induction (Oviedo and Beane, 2009). The zebrafish (Danio rerio) is another model organism that has the ability to fully regenerate many tissues and organs such as the brain, spinal cord, fin, heart, and internal organs. Although zebrafish are also used in cancer research, tumor development in zebrafish is generally lower than in mammals and is only observed at later stages of life, after the age of 1 or 2 years (Feitsma and Cuppen, 2008). In addition, transplantation of human metastatic melanoma cells into zebrafish embryos has shown

* Correspondence to: İstanbul Medeniyet Üniversitesi, Kuzey Yerleşkesi H Blok, Mühendislik ve Doğa Bilimler Fakültesi, Moleküler Biyoloji ve Genetik Bölümü, Ünalan Mah. Ünalan Sk. D100 Karayolu Yanyol, Üsküdar, İstanbul 34700, Turkey.
E-mail address: ekoktem@outlook.com (E. Kubat Oktem).
[1] ORCID ID: 0000–0003-0913–8527

https://doi.org/10.1016/j.compbiolchem.2023.107934
Received 8 June 2023; Received in revised form 13 July 2023; Accepted 18 July 2023
Available online 21 July 2023

that these cells survive, migrate, and proliferate, but are still detectable in adulthood, although they are not cancerous (Lee et al., 2005).

A link between cancer and tissue regeneration has long been established in the literature, with regeneration considered both a cause of cancer and a means to prevent tumor formation (Oviedo and Beane, 2009). The changes in gene expression during wound healing as a regenerative event have already been compared between axolotls and humans (Öktem et al., 2019). Also, comparison of zebrafish brain regeneration with that of two different types of human brain tumors-glioblastoma (GBM) and low-grade glioma (LGG)-at three different time points of injured tissue removal revealed the common and unique molecular processes underlying brain regeneration and brain tumor (Demirci et al., 2022). However, a comprehensive comparison of expressed gene signatures between regenerative and nonregenerative animal models has not yet been performed.

This study is based on the objective of determining the similarities and differences in gene expression between organisms with different regenerative potential. There are studies in the literature that comparatively analyze the regeneration processes of organisms with very different structures (Brockes and Kumar, 2008; Fumagalli et al., 2018; Ricci and Srivastava, 2018). In the study by Fumagalli et al. the genetic activity in regenerating tissues of many different species (from hydra to mouse) was investigated and it was shown that some of the genes and signaling pathways related to regeneration are conserved at the onset of regeneration, even in organisms of very different species (Fumagalli et al., 2018). In addition, there are studies that analyze the differences in gene expression during regeneration between different regenerative species (Dwaraka et al., 2019) or regenerative and nonregenerative organisms at specific time points (Diaz Quiroz et al., 2014; Monaghan et al., 2007; Öktem et al., 2019; Tica and Didangelos, 2018).

We hypothesize that a deeper understanding of the processes controlling cell growth is critical for the development of successful therapeutics in regenerative medicine and cancer. In this study, we aimed to improve the efficacy of existing therapeutics by identifying novel drug molecules related to regeneration and cancer. To this end, we compared publicly available transcriptomic data of spinal cord samples from regenerative and nonregenerative organisms. We then used the comparison of gene expression to reposition anticancer drugs and tested the binding affinities of these drugs using molecular docking techniques. Finally, we tested the anti-cancer activity of our newly developed drugs in vitro (Fig. 1). This study allows us to explore important genes and signaling pathways associated with cancer by approaching them through regeneration, and introduces new candidate anticancer drugs through drug repositioning studies in cancer.

2. Material and methods

2.1. Microarray Data

This study included two groups of organisms, a regenerative and a

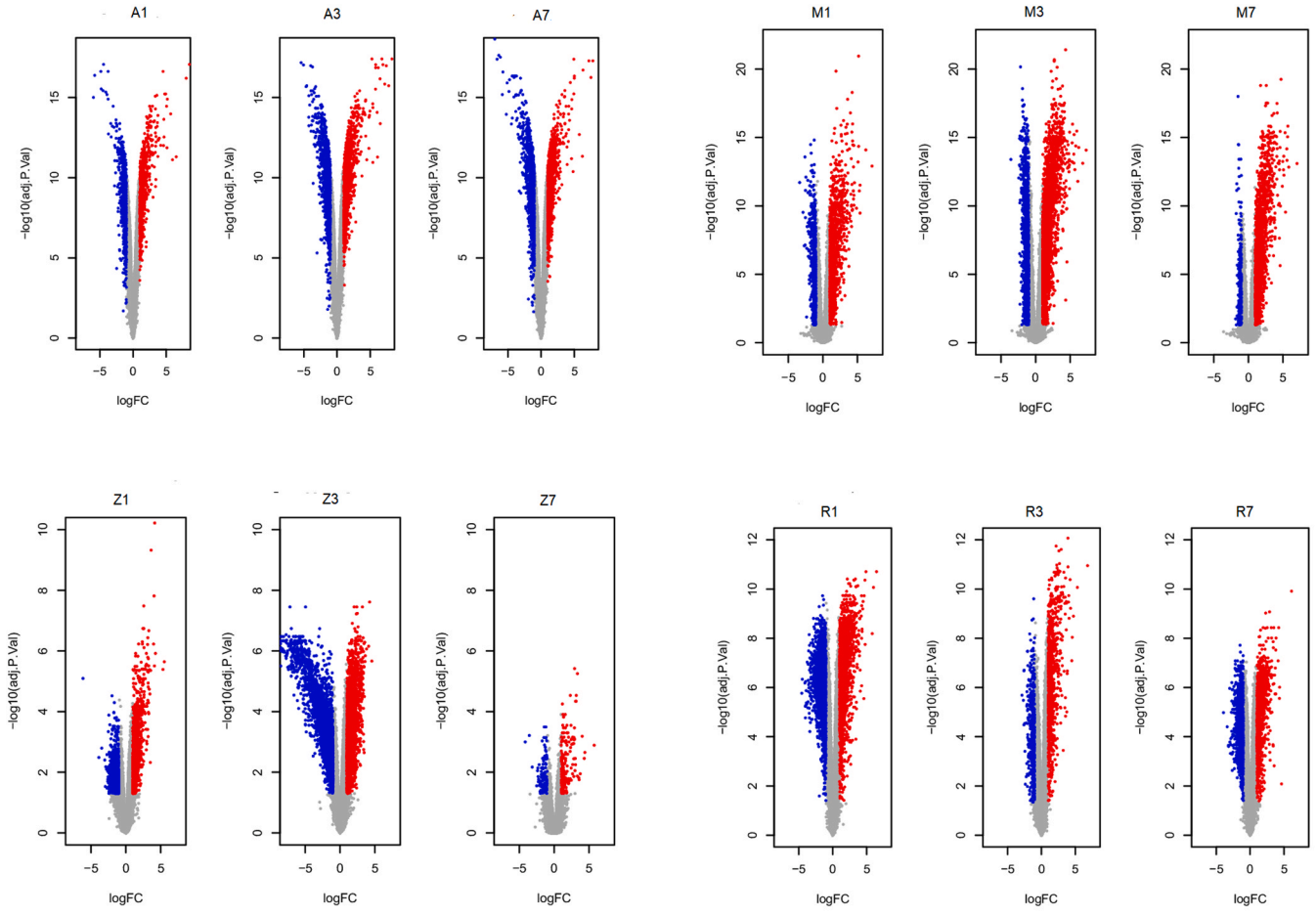

Fig. 1. Volcano plots representing organism-specific DEG profiles at each sampling day. A1:Axolotl spinal cord profile at day 1, A3:Axolotl spinal cord profile at day 3, A7:Axolotl spinal cord profile at day 7, Z1:Zebrafish spinal cord profile at day 1, Z3:Zebrafish spinal cord profile at day 3, Z7:Zebrafish spinal cord profile at day 7, M1: Mice spinal cord profile at day 1, M3: Mice spinal cord profile at day 3, M7: Mice spinal cord profile at day 7,R1:Rat spinal cord profile at day 1, R3:Rat spinal cord profile at day 3, R7:Rat spinal cord profile at day 7. Blue indicates downregulated, red indicates upregulated differentially expressed genes. Gray indicates genes that are not differentially expressed.

nonregenerative group. The regenerative group consisted of datasets from zebrafish and axolotl, while the nonregenerative group included datasets from mouse and rat. The Gene Expression Omnibus (GEO) database contains all of the datasets (Barrett et al., 2013). GSE71934 dataset included 1-month-old axolotl spinal cord samples at day 1 (group A1- 3 samples), day 3 (group A3- 3 samples), and day 7 (group A7- 3 samples) after spinal cord injury, and three intact spinal cord samples as a control group (Sabin et al., 2015). GSE39295 dataset consisted of a 6-month-old early age stage of dorso-ventrally crushed spinal cord zebrafish samples collected at day 1 (group Z1 − 3 samples), day 3 (group Z3–3 samples), day 7 (group Z7–3 samples), and three intact samples as a control group (Hui et al., 2014).

GSE45006, contained thoracic spinal cord rat samples injured by impact compression and collected at day 1 (group R1 - 4 samples), day 3 (group R3 - 4 samples), and day 7 (group R7 - 4 samples), and four intact (sham) samples as a control group (Chamankhah et al., 2013). Mouse dataset GSE5296 (unpublished data), consisted of injured spinal cord samples collected at the impact site at day 1 (group M1 - 3 samples), day 3 (group M3 - 3 samples), and day 7 (group M7 - 3 samples), as well as two intact (sham) samples as a control group (Table 1).

2.2. Differential gene expression (DEG) analysis

Data from the Agilent dataset (GSE39295) were preprocessed using the GEOquery package (Sean and Meltzer, 2007) and quantile normalization was performed. The Affy package (Gautier et al., 2004) was used to read the raw data from the Affymetrix datasets into R statistical software (version 4.3.0) and data were normalized using Robust Multi-Array Average (RMA) (Bolstad et al., 2003) of R Bioconductor (version Rx64 3.17) (Gentleman et al., 2004). The Linear Models for Microarray Data (LIMMA) (Smyth et al., 2005) package was applied to compare the normalized expression levels of the genes and to determine the differentially expressed genes (DEGs). Each organism was statistically matched to its own intact sample group as a control at each sampling day. False discovery rates were controlled using the Benjamini-Hochberg procedure. A log2FC cut-off value of 0.585 and an adjusted p-value of <0.05 were used to determine the statistical significance of the differentially expressed genes. After analyzing the DEGs for each organism, human orthologs of the DEGs for each organism were sought to compare the gene expression profiles of these organisms. The IDs of the axolotl microarrays were linked to the human orthologs using the GEOquery package. The DEGs of the other three organism species were aligned to human othologs using Ensembl:Biomart (Ensembl 106: Apr 2022) (Smedley et al., 2015). The GRCm39 (Genome Reference Consortium Mouse Build 39), mRatBN7.2 (rat genome assembly), and GRCz11 (Genome Reference Consortium Zebrafish Build 11) were used to annotate the human orthologous genes for mouse, rat, and zebrafish genes respectively. The human GRCh38.p13 (Genome Reference Consortium Human Build 38 patch release 13) genome version was used to obtain human orthologous genes. For each organism, the corresponding genome version was selected. The list of external references ID was filtered by gene name. Human gene name, and human gene stable ID were selected as attributes to find the human orthologs. The heatmap of the DEGs was generated using the R package pheatmap (Kolde, 2012).

Table 1
GEO Datasets Used in the Study.

GEO #	Organism	Sample Subsets	Array
GSE71934	Ambystoma mexicanum (Axolotl)	3 uninjured axolotl SC samples (control) 3 axolotl SC samples (DPI 1) 3 axolotl SC samples (DPI 3) 3 axolotl spinal cord samples (DPI 7)	GPL15153 Affymetrix Ambystoma mexicanum AMBY_002 20k array
GSE39295	Danio rerio (Zebrafish)	3 uninjured zebrafish SC samples (control) 3 zebrafish SC samples (DPI 1) 3 zebrafish SC samples (DPI 3) 3 zebrafish spinal cord samples (DPI 7)	Agilent-021643 GIS Zebrafish Array ver1.1_custom layout
GSE45006	Rattus norvegicus (rat)	4 uninjured rat SC samples (control) 4 rat SC samples (DPI 1) 4 rat SC samples (DPI 3) 4 rat SC samples (DPI 7)	GPL1355 [Rat230_2] Affymetrix Rat Genome 230 2.0 Array
GSE5296	Mus musculus (mouse)	2 uninjured mouse SC samples (control) 3 mouse SC samples (DPI 1) 3 mouseSC samples (DPI 3) 3 mouse SC samples (DPI 7)	GPL1261 [Mouse430_2] Affymetrix Mouse Genome 430 2.0 Array

GEO: Gene Expression Omnibus, SC: spinal cord, DPI: Days post injury

2.3. Functional enrichment analysis

Metascape 3.5 (Zhou et al., 2019) was used to perform functional and pathway enrichment analyses to find functional annotations (i.e., biological processes and molecular pathways) that were significantly associated with DEGs. First, we identified all statistically enriched terms based on the default selection under the Express Analysis option of the Metascape tool. Filtering was based on accumulative hypergeometric p-values and enrichment factors. The rest of the statistically significant terms were then clustered in a tree hierarchically based on the statistical kappa correlations between their gene memberships. The annotation sources used were the Reactome (Fabregat et al., 2016), Gene Ontology (GO) Biological Processes (Ashburner et al., 2000; Carbon et al., 2021), and KEGG (Kanehisa et al., 2008) databases.

2.4. Drug repositioning using DEGs

L1000CDS2 (LINCS L1000 characteristic direction signature search engine) was performed to find potential drug candidates (http://amp.pharm.mssm.edu/L1000CDS2). L1000CDS2 is a search engine that allows discovery of a consensus of L1000 small molecules that fit user-defined signatures (Duan et al., 2016) (i.e., up- or down-regulated genes). The differentially expressed (DE) genes in these profiles were determined using the characteristic direction method (Clark et al., 2014). To investigate the predicted target genes among the repositioned drugs, we applied a strategy similar to that previously used (Öktem et al., 2019). Analyses were performed in two scenarios to find drugs that could potentially reverse gene expression states of nonregenerative organisms or mimic gene expression states of regenerative organisms. The first scenario involved reversing upregulated gene expressions and downregulated gene expressions in nonregenerative organisms. The second scenario was created by mimicking upregulated gene expressions and downregulated gene expressions in regenerative organisms. Drug information was retrieved from NCBI PubChem (Kim et al., 2019). We found chemical and physical properties, biological activities, safety and toxicity information and patents by searching for the names of repositioned drugs.

2.5. Identification of predicted target genes for repositioned drugs

To investigate the predicted target genes among the repositioned drugs, we applied a strategy similar to that previously used (Kubat Oktem et al., 2022; Oktem and Yazar, 2022). The most significant drug molecules were filtered out for our investigation using the Search Tool for Interactions of Chemicals (STITCH, stitch.embl.de), a protein-compound interaction database comprising 430,000 chemicals and 9.6 million proteins (Szklarczyk et al., 2016). The screening compounds were aimed to recover along with their corresponding predicted target genes. STITCH database also revealed an analysis of the enrichment of predicted target genes from the KEGG database in default (Kanehisa et al., 2008).

2.6. Construction of the Protein-Protein Interaction (PPI) networks around predicted target genes

The PPI network was constructed using the predicted target genes for the repositioned compounds. BioGrid (version 4.4.202.10) (Oughtred et al., 2019) provided the PPI data, and Cytoscape (version 3.9.0) (Shannon et al., 2003) was used to visualize the networks. Modules of PPI networks were displayed using the MCODE plugin (Bader and Hogue, 2003).

2.7. Molecular Docking Analysis

Molecular docking analysis was performed using AutoDock Vina 1.2.0 (Eberhardt et al., 2021) to analyze the associations between drugs and the corresponding proteins and to measure the binding energy of the protein-ligand complex. The 3D protein structures (PDB IDs) of the module genes were downloaded from the Protein Data Bank (PDB) of the Research Collaboratory for Structural Bioinformatics (RCSB) (Berman et al., 2000). The 3D drug structures were downloaded from NCBI PubChem (Kim et al., 2019) and DrugBank (Wishart et al., 2018). The 3D crystal structures were cleaned of solvent molecules, water, and other ligands, and the dimensions of the lattice boxes for the targets were changed to match the x, y, and z coordinates for all proteins. Then, the pdb files of the proteins were converted to PDBQT format after polar hydrogens and charges were added to the protein structures. Binding pocket prediction analysis was performed in CASTp 3.0 web browser (Tian et al., 2018), and the gridbox of molecular docking analysis for search space was adjusted to the region according to the binding pocket prediction. The ligand bonds were permitted unrestricted rotation, whereas the protein remained in a fixed state. Molecular docking procedure were applied to all available protein-ligand couples with default parameters of AutoDock Vina 1.2.0 on Windows 10 platform (64-bit) with ASUS FX503VD personal computer (Intel Core Intel(R) Core (TM) i7–7700Q CPU Processor 2.80 GHz, 8 GB memory). The ligands exhibiting the lowest binding energies were chosen in order to assess the docking results. Nine modes were used to predict the binding affinity between each protein-drug complex. AutoDock Tools (1.5.7) (Morris et al., 2009) was used to create charts showing statistically significant results.

2.8. Cell viability analysis and IC50 calculations

The prostate cancer cell line PC3 was used to confirm the anti-cancer potential of the proposed drugs by in vitro analysis. PC3 cells were cultured in RPMI cell culture media containing 10% FBS and 1% P/S at 37 °C and 5% CO2. For the viability assay, PC3 cells were seeded in 96-well plates at a cell density of 6000 cells/well. After 24 h, the cells were treated with increasing concentrations of each small compound. Cells were incubated with the small compounds for 48 h and cell viability was determined by crystal violet staining. Cells were washed with PBS and stained with 0.5% crystal violet in ethanol. Methanol was used to dissolve the crystal violet from the cells, and absorbance was measured at 590 nm in a multiplate reader. Experiments were repeated at least three times, with each experiment performed in triplicate. IC50 values for each small compound were calculated using GraphPad Prism version 8.0.0 for Windows, GraphPad Software, San Diego, California USA, www.graphpad.com.

2.9. 3D cell culture

PC3 cells were seeded in 96-well plates with low attachment at a density of 2000 cells/well. They were allowed to form spheroids for 48 h. The spheroids were treated twice with small compounds 48 h apart. After 48 h of the second treatment, the viability assay was performed. Briefly, the spheroids were dispersed with a pipette and MTS (Abcam) was added 1/10 of the culture medium. Cells were incubated with the MTS reagent for 3–4 h and absorbance was measured at 490 nm in a multiplate reader.

2.10. Statistical analysis

All statistical analyses were listed and described in each section. The Linear Models for Microarray Data package (LIMMA) (Smyth et al., 2005) uses the moderated t test to calculate the p value for the differentially expressed genes (DEGs) (Smyth, 2004). We used the Benjamini-Hochberg procedure to decrease the false discovery rate. In the L1000CDS2 tool, the p-value of the test is calculated using Fisher's exact test (Duan et al., 2016). The viability of the cells and spheroids against the drugs was analysed using student t-test.

3. Results

3.1. DEG (Differential gene expression) profiles in regenerative (Axolotl, Zebrafish) and nonregenerative (Rat, Mouse) groups

The changes in gene expression during spinal cord regeneration in the data sets were analyzed, and volcano plots were generated for each day of sampling before their human orthologs were examined (Fig. 1). Downregulated and upregulated orthologous genes were equally distributed in the regenerative and nonregenerative groups on all sampling days (Table 2).

3.2. Analysis of gene expression alteration between regenerative and nonregenerative groups

A total of 60 different DEGs showed a reverse expression pattern between 2 groups (downregulated in axolotl and zebrafish as regenerative group, upregulated in mice and rat as nonregenerative group, or vice versa) during the 7-day period (Fig. 2 and Supplementary Tables 1–3). At day 1, a total of 28 different DEGs showed a reversed expression pattern between regenerative and nonregenerative groups, of which 23 were upregulated in nonregenerative organisms and downregulated in regenerative organisms, whereas the remaining 5 were reversed. On day 3, the number of DEGs showing a reversed expression pattern between the two groups increased to 50, of which 43 were upregulated in nonregenerative organisms and downregulated in regenerative organisms, whereas 7 were downregulated in nonregenerative organisms and upregulated in regenerative organisms. By day 7, the reverse pattern between the two groups completely resolved. 16 genes, namely *MCM7, TK1, SMC4, KIF11, RRM2, MCM2, CCNA2, NASP, KPNA2, MCM4, CDC20, PCNA, TOP2A, RRM1, PPP1R3B, POLE2* were the common genes of day 1 and day 3 that were downregulated in regenerative organisms, whereas they were upregulated in nonregenerative organisms. *CBLN1* and *CHGA* were the two common genes of day 1 and day 3 that were upregulated in regenerative organisms, while they were downregulated in non-regenerative organisms. Throughout the 7-day period, a total of 50 genes were upregulated in the nonregenerative group and downregulated in the regenerative group,

Table 2
Number of Differentially Expressed Genes of Human Orthologous Genes.

Regeneration Status	Organism	Total # of DEGs	# of upregulated DEGs	# of downregulated DEGs	Threshold for adj. p-value	Threshold for fold change
Regenerative	A1	6784	1119	1353	0.05	1.5
Regenerative	A3	7435	1279	1874	0.05	1.5
Regenerative	A7	8796	1545	1612	0.05	1.5
Regenerative	Z1	1209	556	483	0.05	1.5
Regenerative	Z3	2405	995	1128	0.05	1.5
Regenerative	Z7	114	77	28	0.05	1.5
Nonregenerative	M1	5607	1843	1924	0.05	1.5
Nonregenerative	M3	6297	2928	2348	0.05	1.5
Nonregenerative	M7	4692	1933	1246	0.05	1.5
Nonregenerative	R1	7918	2536	1688	0.05	1.5
Nonregenerative	R3	6448	1766	930	0.05	1.5
Nonregenerative	R7	6269	1617	1150	0.05	1.5

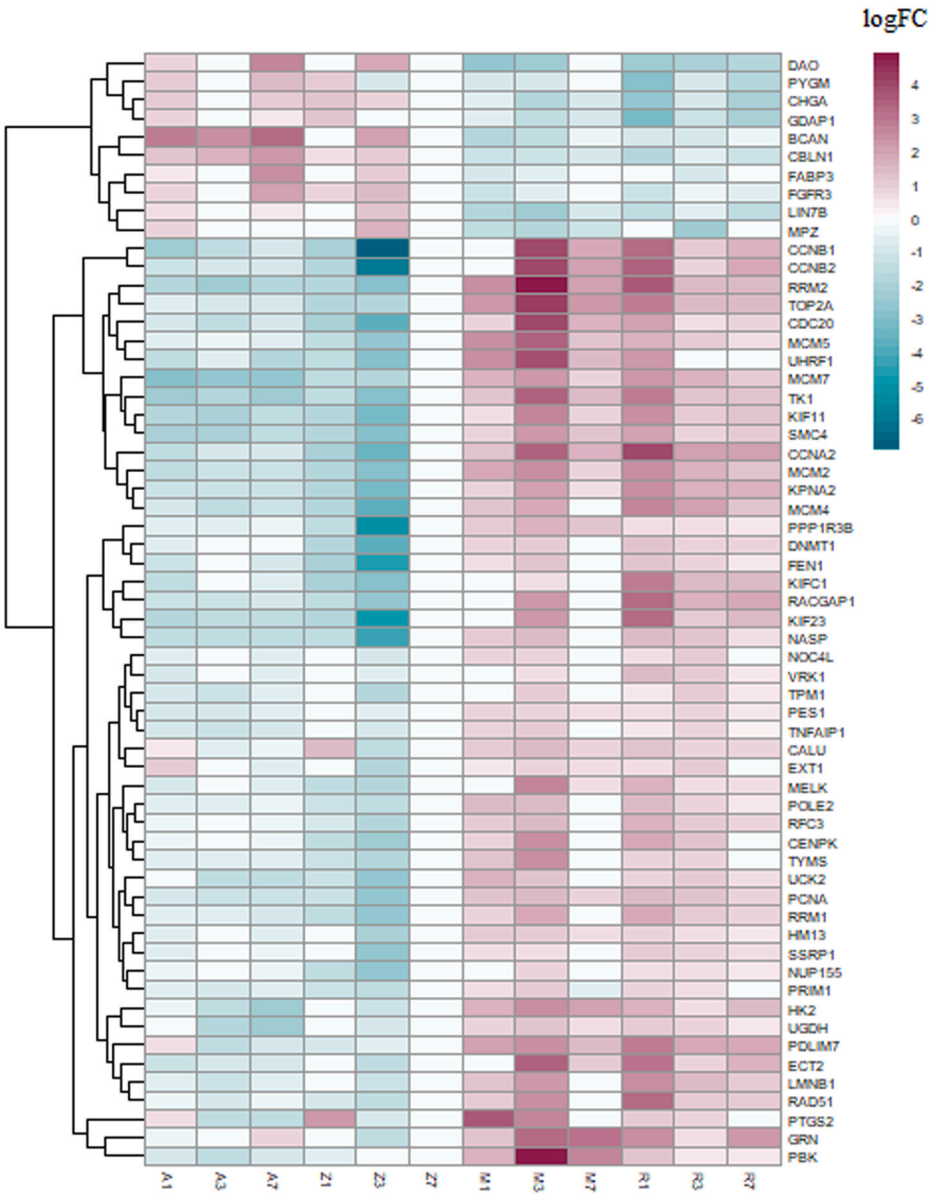

Fig. 2. Heatmap of 60 gene signatures showing an organism-specific reverse expression profile.

whereas 10 genes were downregulated in the nonregenerative group and upregulated in the regenerative group.

3.3. Biological interpretation of reversely expressed gene signatures

The 60 DEGs were additionally examined for their role in molecular signaling pathways and bioprocesses. Most pathways were associated with the mitotic phases of the cell cycle, DNA replication, DNA conformational changes, DNA repair, and cancer (Fig. 3 and Supplementary Table 4).

3.4. Analysis of drug repositioning

Drugs with a score greater than 0.5 in the L1000CDS2 database were evaluated for cancer treatment. We present these drugs, 14 in total, in the Supplementary Table 5. Among these drugs, etoposide is an FDA-approved anticancer drug (Montecucco et al., 2015), so we excluded this drug from our further analysis.

3.5. Predicted target genes for the repositioned molecules

Screening of drug-associated processes using the Search Tool for Interactions of Chemicals (STITCH) found predicted target genes for 5 of the 13 remaining repositioned anticancer drugs. These drugs with their predicted target genes in red are shown in Fig. 4. The protein-protein interaction network with the remaining 8 molecules either did not have significantly higher than expected interactions or could not be found in the STITCH database (these drugs have not yet been studied, and STITCH may not yet know how they interact with each other).

The predicted target genes for 5 screening drugs, namely quinacrine hydrochloride, BMS-754807, cucurbitacin I, tyrphostin AG 1478, and PHA-793887, were mainly enriched with the largest number of genes in cancer pathways (Supplementary Table 6).

3.6. Analysis of the Protein-Protein Interaction (PPI) networks around predicted target genes

Quinacrine hydrochloride, one of the repositioned drugs, shared one gene - *RAD51* - with our DEG list, while PHA-793887 shared two genes - *CCNA2* and *CDC20* - with our DEG list. The other three drugs shared no genes in common with our DEG list. To include genes of that might be related in some way to the repositioned drugs as downstream or upstream components of the proposed target genes, we attempted to create PPI networks for the target genes of BMS-754807, cucurbitacin I and tyrphostin AG 1478. Modules were found using the MCODE plugin of Cytoscape by locating clusters within each network. The cut-off value for the degree and the cut-off value for node score were set to 2 and 0.2, respectively. The K-Core parameter of 2 and the Max. Depth of 100 were also used to access densely networked modules. The clusters of each drug are shown in Supplementary Figure 1 and Supplementary Table 7.

3.7. Molecular docking between PPI network module elements and repositioned drugs

The predicted target gene for quinacrine hydrochloride, *RAD51*, the predicted target genes of PHA-793887, *CCNA2* and *CDC20*, and genes of each cluster from ppi analysis of BMS-754807, cucurbitacin I and tyrphostin AG 1478 were used for molecular docking analysis. The PDB IDs of the protein structures for the corresponding proteins were found in the RSCB Protein Data Bank (PDB). Autodock Vina 1.2.0 was used to assess the binding affinity values between the drug candidates and the module genes and to sort them in ascending order (from strong to weak binding) (Table 3).

Three of the repositioned drugs, namely cucurbitacin I, BMS-754807, and PHA-793887, exhibited protein-ligand pairs with binding affinities of < -8 kcal/mol with the corresponding proteins, which is considered a good value in the literature (Gurung et al., 2016; Jabir et al., 2021). The molecular docking results of these drugs with their proteins are shown in Fig. 5.

3.8. Analysis of cell viability in 2 and 3D cell culture in response to three small compounds

IC50 values were calculated for each compound in PC3 cells. Cucurbitacin I (150 nM) (Fig. 6a) and PHA- 793887(712 nM) (Fig. 6b) exerted their effects in the nanomolar range, while BMS-754807 (2.76 μM) (Fig. 6c) exerted its effects in the micromolar range.

Spheroid models have become an important component of in vitro cancer models because they better mimic in vivo conditions. For PC3 cells, ultra-low attachment plates were used to form spheroids, and the small compounds were administered at two different concentrations. Viability results showed that although cucurbitacin I acted at lower concentrations in the 2D cell culture, it was less effective in the 3D spheroids (Fig. 7a, b, and g). PHA-793887 and BMS-754807 were even more effective in spheroids than in 2D cell culture (Fig. 7c, d, e, and f). Even below IC50 levels, they showed profound antiproliferative effects in spheroids with marked cell apoptosis (Fig. 7h and i).

4. Discussion

In this study, the changes in gene expression during spinal cord regeneration were examined in the datasets of regenerative organisms and nonregenerative organisms with injured tissues on three collection days and matched with those of control samples in each organism to analyze possible genes linking the regeneration process to cancer. A total of 60 DEGs showed a reversed expression profile and the association of these genes with enriched carcinogenesis pathways is consistent with the literature (Villa et al., 2019). Similarly, the predicted target genes for

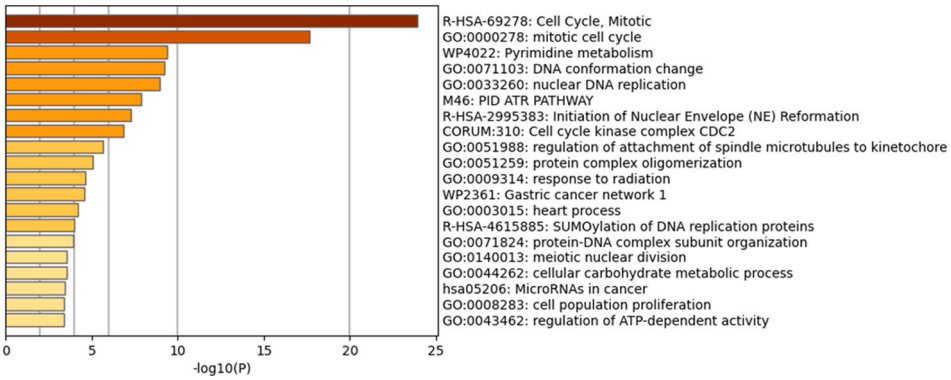

Fig. 3. Pathway enrichment results of the DEGs with reverse expression profile, the significance of the pathways is displayed by darker colors.

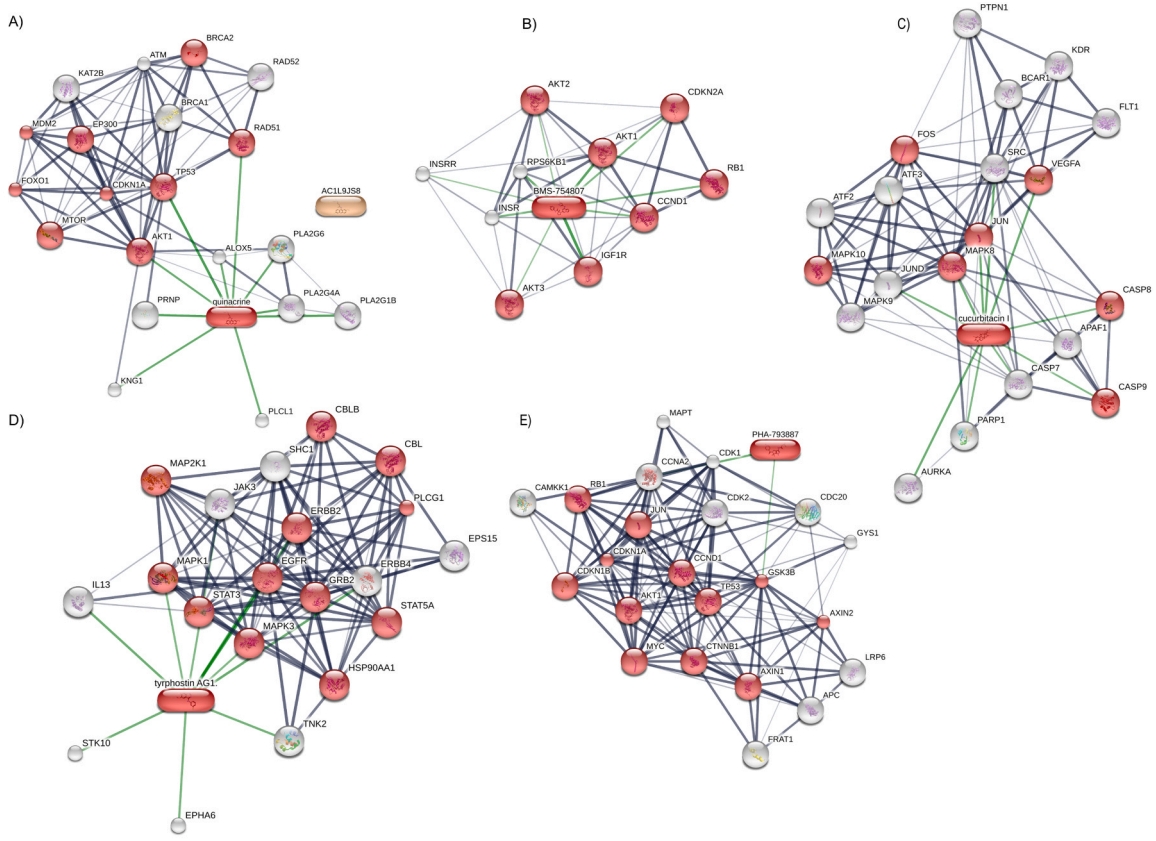

Fig. 4. Predicted target genes of 5 screening drugs based on Search Tool for Interactions of Chemicals. (A) quinacrine hydrochloride, (B) BMS-754807, (C) cucurbitacin I, (D) tyrphostin AG 1478, (E) PHA-793887. Red hubs indicate the repositioned drug with its predictted target genes in cancer pathways.

Table 3
Predicted binding affinity between drug candidates and module genes.

Drug	Protein name	PDB identifier	Binding affinity (kcal/mol)
BMS-754807 (DB15399)	RPS6KB1	3WF7	-9
cucurbitacin I	PTPN11	2shp	-9
BMS-754807 (DB15399)	EP300	3BIY	-8.6
PHA-793887 (DB12686)	CCNA2	2cch	-8.5
cucurbitacin I	MAPK9	7cml	-7.9
PHA-793887(DB12686)	CDC20	4gga	-7.6
Tyrphostin AG 1478	ERBB4	3bce	-7.6
cucurbitacin I	KDR	1YWN	-7.4
cucurbitacin I	EP300	3BIY	-7.4
cucurbitacin I	MAPK8	2xrw	-7.3
cucurbitacin I	CREBBP	3p1f	-7.3
Tyrphostin AG 1478	ERBB2	1s78	-7.1
cucurbitacin I	FLT1	4ckv	-7.1
BMS-754807 (DB15399)	AKT1	2UVM	-6.8
Tyrphostin AG 1478	CBL	1yvh	-6.8
cucurbitacin I	ATF2	1bhi	-6.6
QUINACRINE HYDROCHLORIDE (DB01103)	RAD51	1N0W	-6.5
cucurbitacin I	VEGFA	1flt	-6.4
Tyrphostin AG 1478	GRB2	1bmb	-6.1
Tyrphostin AG 1478	SHC1	4xwx	-6.1
Tyrphostin AG 1478	PLCG1	4fbn	-6
cucurbitacin I	JUND	5vpe	-6
cucurbitacin I	JUN	1jnm	-5.5
Tyrphostin AG 1478	EGFR	1m17	-4.7
Tyrphostin AG 1478	ACTB	NA	NA
Tyrphostin AG 1478	HSPA5	NA	NA
cucurbitacin I	ATF3	NA	NA

NA: Not available (3D protein structure is not available)

five screening drugs were mainly enriched in carcinogenesis pathways. This result is also consistent with our research goal, which is to develop new drugs targeting cancer-related pathways to cure cancer.

The repositioned molecules found in this study have the potential to mimic the anticancer behavior of regenerative organisms and reverse the cancer behavior of nonregenerative organisms. Among these molecules, cucurbitacin I is a STAT3 inhibitor and is used in traditional medicine for its anti-inflammatory, antipyretic, and analgesic properties. Cucurbitacin I has been shown to kill cancer cells by blocking a number of signaling pathways, including the Janus kinase (JAK)/STAT3, the PI3K/AKT/p70S6K, the Notch signaling pathway (Dandawate et al., 2020), and the serine/threonine protein kinase PAK1 (PAK1)/PAK4 pathway (Nguyen et al., 2016; Yang et al., 2017). In the literature, the anticancer agent cucurbitacin I was reported to have potent anticancer activity on ovarian cancer (Li et al., 2020), colon cancer (Dandawate et al., 2020), and non-small cell lung cancer cells (Ni et al., 2018). Its activity as a STAT3 inhibitor has been confirmed in prostate cancer. At a concentration of 0.5 microM, cucurbitacin I inhibited STAT3 activity in Du-145 cells, but no effects on viability were observed (Chau and Banerjee, 2008). There is no other study in the literature on the effect of cucurbitacin I in prostate cancer. However, numerous studies have reported the antiproliferative effects of other cucurbitacins such as cucurbitacin E, D, or B in prostate cancer cells (Alafnan et al., 2022; Duncan et al., 1996; Gao et al., 2014b; He et al., 2017). Cucurbitacin D has the most similar chemical structure to cucurbitacin I. In the study by Sikander et al., cucurbitacin D showed similar antiproliferative effect in PC3 cells as cucurbitacin I in our study. At concentrations of 0.1 and 0.5 microM, cucurbitacin D inhibited proliferation and induced apoptosis. The mechanism of action was defined via glucose metabolism by targeting GLUT1 (Sikander et al., 2019).

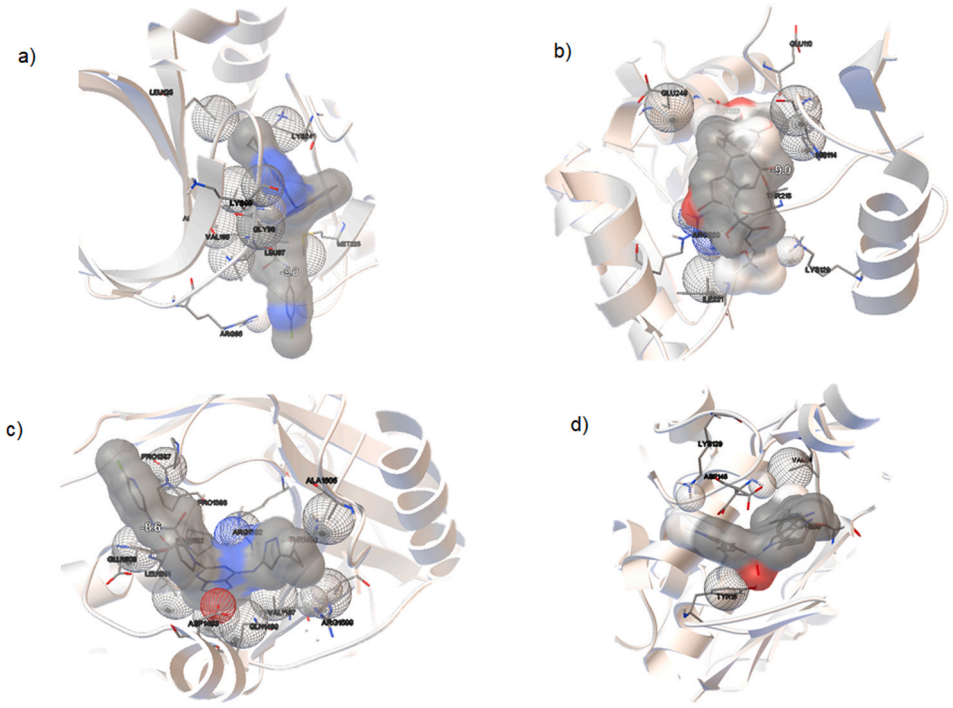

Fig. 5. Three- dimensional structures of the repositioned molecule-protein with highest binding affinities of < −8 kcal/mol based on Autodock Vina. a) BMS-754807- RPS6KB1; b) cucurbitacin I- PTPN11; c) BMS-754807 - EP300; d) PHA-793887- CCNA2.

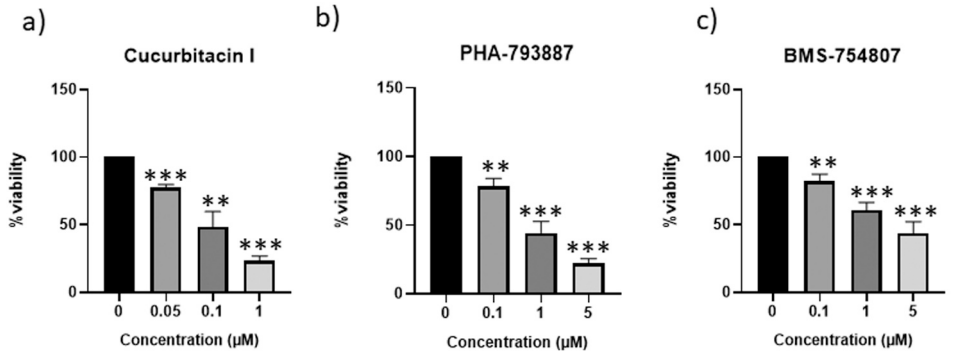

Fig. 6. The dose dependent response to compounds in PC3 cells. The cells were treated with increasing concentrations of three small compounds for 48 h. a) Cucurbitacin I, b) PHA-793887, c) BMS-754807. %Viability was calculated by comparing treatment groups to control. * $p < 0.05$, ** $p < 0.01$ and ***$p < 0.001$ by student t-test.

According to the molecular docking results of our study, the highest binding affinity was observed between cucurbitacin I and PTPN11 protein (−9 kcal/mol) (Table 3). PTPN11, also known as SHP2, was the first protein tyrosine phosphatase to be recognized as carcinogenic, and it is found in a wide variety of cells and tissues (Chan and Feng, 2007). PTPN11 regulates a wide range of intracellular activities, including apoptosis, invasion, mitogenic activation, senescence, tumor cell proliferation, differentiation, invasion, and metastasis (Miyamoto et al., 2008; Yang et al., 2013; Zhang et al., 2015). In addition, *PTPN11* has been identified as a critical oncogene that is well studied in various malignancies, including melanoma (Hill et al., 2019) and breast cancer (Aceto et al., 2012). A pan-cancer analysis of *PTPN11* showed that there is an association between *PTPN11* expression and prognosis, suggesting that this protein could be a potentially important marker for cancer treatment (Cao et al., 2022).

The transmembrane tyrosine kinase growth factor receptor known as insulin-like growth factor-I receptor (IGF-1R) is critical for the development and maintenance of the transformed phenotype; when activated, cancer cells undergo mitogenesis and survive (Baserga et al., 1994; Pollak et al., 2004; Sachdev and Yee, 2007). Insulin receptor family kinases are effectively and irreversibly inhibited by the drug BMS-754807. Several types of human malignancies, including mesenchymal, epithelial, and hematopoietic tumor cell lines, are treated with this drug (Carboni et al., 2009a). BMS-754807 has been studied in many different cancer types in vitro and in vivo (Carboni et al., 2009b; Halvorson et al., 2015; Kolb et al., 2014). These studies were also followed up in clinical trials. However, due to adverse events, most clinical trials were terminated. However, the studies in prostate cancer are very limited. Dayyani et al. investigated the effect of BMS-754807 on prostate cancer cells. No IC50 value was reported for PC3, but concentrations of 2 and 5 microM were used for anti-proliferation and anti-apoptosis studies, respectively (Dayyani et al., 2012). These concentrations are consistent with the IC50 value we determined. Despite the initial failure of BMS-754807 in clinical trials, many studies are exploring the effect of

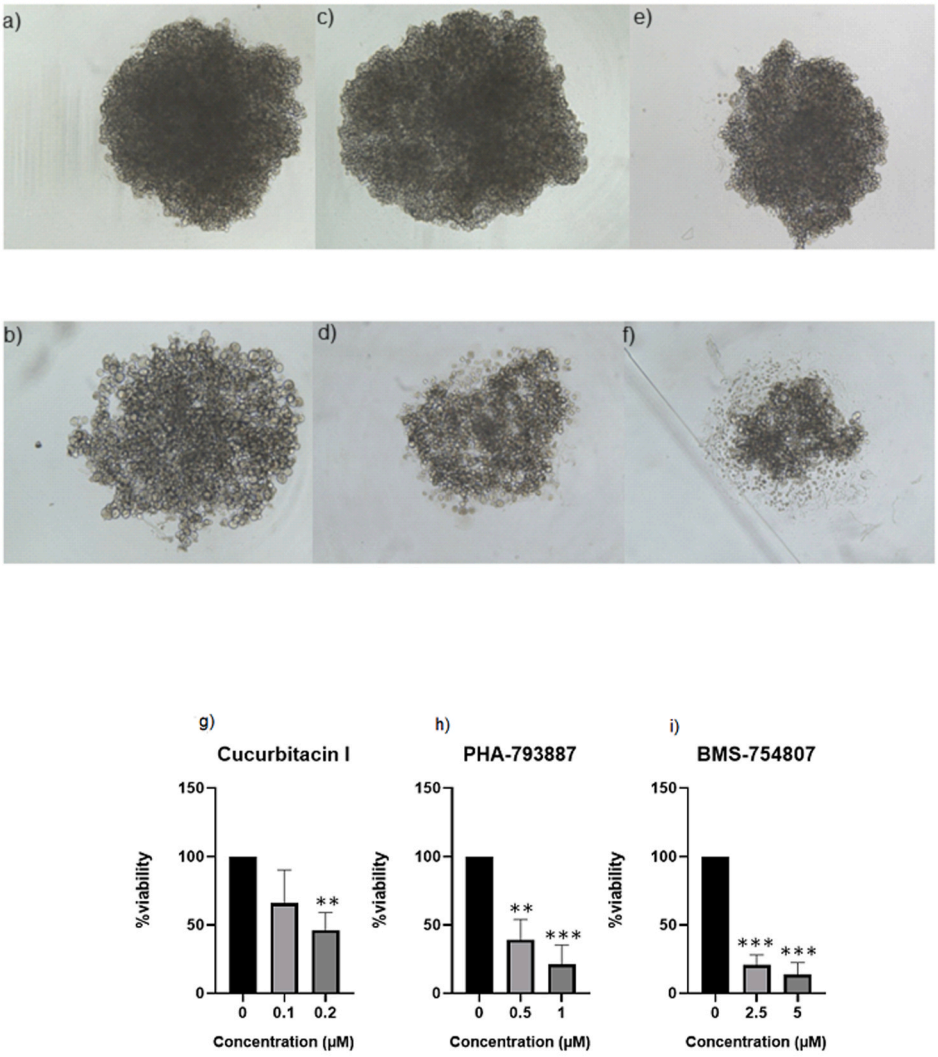

Fig. 7. The effect of compounds in PC3 spheroids. After formation of spheroids, the compounds were administered twice with 48 h interval at indicated concentrations. a) Control spheroid, b) Cucurbitacin I treated spheroid (0.2 μM), c) Control spheroid, d) PHA-793887 treated spheroid (1 μM), e) Control spheroid. f) BMS-754807 treated spheroid (5 μM), g) Dose dependent viability of 3D spheroids after Cucurbitacin I treatment, h) Dose dependent viability of 3D spheroids after PHA-793887 treatment, i) Dose dependent viability of 3D spheroids after BMS-754807 treatment.

combination therapies with BMS-754807 (Molecule et al., 2020; Shen et al., 2019). Our study may lead the way for combination trials of BMS-754807 in prostate cancer.

The molecular docking results of our study showed that BMS-754807 has a binding affinity to RPS6KB1 and EP300 with − 9 kcal/mol and-8.6 kcal/mol, respectively (Table 3). RPS6KB1 ribosomal protein S6 kinase B1, known also as P70S6K, is a serine/threonine kinase that is activated downstream of the PI3K/AKT/mTOR pathway (Jimeno et al., 2022), which is frequently active in triplenegative breast cancer (TNBC) patients (Pérez-Tenorio et al., 2002; Sohn et al., 2013). P70S6K is upregulated in TNBC cell lines and clinical samples, and it has been suggested as a modulator of carcinogenesis and metastasis (Akar et al., 2010; Berman et al., 2017; Janaki Ramaiah et al., 2014; Razaviyan et al., 2018). In human esophageal carcinoma, increased expression of RPS6KB1 in tumor tissues predicted a worse prognosis with a lower survival rate (Wang et al., 2021). The other protein, EP300 (E1A-binding protein p300) is a histone acetyltransferase responsible for chromatin remodeling to regulate transcription (Eckner et al., 1994). This protein is critical for the control of differentiation and proliferation (Gayther et al., 2000). As a result, EP300 mutations have been linked to cancer (Bi et al., 2019; Huang et al., 2021). The correlation between EP300 mutations and genome instability in 11 cancers (skin cutaneous melanoma (SKCM), lung adenocarcinoma (LUAD), urothelial bladder carcinoma (BLCA), UCEC (uterine corpus endo-metrial carcinoma), HNSC (Head and neck squamous cell carcinoma), esophageal carcinoma (ESCA), CESC (cervical squamous cell carcinoma), stomach adenocarcinoma (STAD),breast invasive carcinoma (BRCA), liver hepatocellular carcinoma (LIHC), and colon adenocarcinoma (COAD) has shown that EP300 mutations are associated with increased genomic instability, making them a predictive biomarker for response to cancer treatment (Chen et al., 2021).

Cyclin-dependent kinases (cdk), typically differentially expressed in human malignancies, are responsible for regular cell cycle control (Alzani et al., 2010). Because cdk-related proteins play a role in human cancers, numerous cdk inhibitors have been developed and are currently being investigated in clinical trials (Malumbres and Barbacid, 2009). PHA-793887 is a cdk inhibitor that inhibits cell proliferation in a number of solid tumor cell lines (Brasca et al., 2010a) and acute leukemias both in vitro and in vivo (Alzani et al., 2010). PHA-793887 is a pan-CDK inhibitor developed in 2010 (Brasca et al., 2010b). The IC50 concentration for PC3 cells reported in this very first study was very similar to the IC50 value obtained in our study (0.601 versus 0.71). The Phase I clinical trial of PHA-793887 evaluated the pharmacokinetics of the drug candidate. The adverse side effects such as hepatotoxicity preclude further development of the drug (Massard et al., 2011).

PHA-793887 has also been studied in cell lines and organoid models of prostate cancer. In this study, organoids from abireterone-resistant patients were used. Therefore, the drug concentration was 5–20 microM, which is much higher than the IC50 value we determined (Qin et al., 2022). According to the results of a recent bioinformatic analysis

in gastric cancer and osteosarcoma, PHA-793887 was found to be an important drug candidate in cancer (Li et al., 2023; Wu et al., 2021). Our study also showed that PHA-793887 was effective in 3D models at lower concentrations. In light of these studies and our study, re-evaluation of this drug in cancer treatment at lower doses is warranted.

According to the molecular docking analysis of our study, the binding affinity of PHA-793887 to CCNA2 protein is − 8.5 kcal/mol (Table 3). CCNA2 (CyclinA2) is a member of the highly conserved cyclin family and is found in almost all human tissues (Ko et al., 2013). It plays a crucial role in embryonic cells and exerts critical functions in cell cycle control at the G1/S and G2/M transitions (Arsic et al., 2012). CCNA2 is upregulated in numerous cancers, suggesting that it may play a role in carcinogenesis (Uhlen et al., 2010). It has also been suggested that CCNA2 plays an important role in metastasis and epithelial-mesenchymal transition (EMT) (Bendris et al., 2012). CCNA2 has shown a strong prognostic power in patients with estrogen receptor-positive (ER +) breast cancer and is proposed as a biomarker for this disease (Gao et al., 2014a). Moreover, the expression of *CCNA2* is much higher in colorectal tissues compared with normal tissues, and a decrease in *CCNA2* leads to a slowing of cell cycle progression and apoptosis, suggesting that CCNA2 can be used as a new diagnostic indicator and a guide for the treatment of this type of cancer (Gan et al., 2018).

This study has several limitations, one of which is its dependence on adequate sample size; the small size of the data sets we used limits the generalizability of our results. Although the number of samples was sufficient for statistical analysis, the stringency of the available datasets limited the analyses to datasets with a small sample size, and each organism was represented by a single dataset. In vitro experiments were also limited to a single cell line and were not confirmed in vivo. However, the promising results of the 3D spheroid experiments warrant further investigation and validate the concept of the study. Repeating the work with independent datasets from multiple platforms with more samples or examining the results with other types of omics data, such as metabolomics or proteomics, performing in vitro assays in different cancer cell models and in vivo experiments and analysing the toxicity and potential side effects of these compounds would strengthen our findings.

5. Conclusion

This study helps to evaluate mechanisms and gene signatures that either hinder or trigger cancer and to propose three anticancer drugs by establishing a link between regeneration and tumorigenesis. We anticipate that these potential drug candidates will contribute to the development of innovative and definitive treatments to cure cancer. Future efforts to find out the mechanisms associated with these gene signatures and the effects of the repositioned drugs would allow researchers to develop therapeutic strategies to fight cancer. Our results also provide new perscpective for use of these anticancer drugs and pave the way for in vivo and pre-clinical testing of these drugs in prostate cancer.

CRediT authorship contribution statement

EKO: Conceptualization, Methodology, Formal analysis, Investigation, Writing – original draft, Writing – review & editing, Visualization. **UD:** Conceptualization, Methodology, Formal analysis, Investigation, Writing – original draft, Writing – review & editing, Visualization. **MY:** Methodology, Formal analysis, Investigation, Writing – original draft, Writing – review & editing, Visualization. **KYA:** Conceptualization, Writing – review & editing, Supervision.

Declaration of Competing Interest

The authors declare that they have no known competing financial interests or personal relationships that could have appeared to influence the work reported in this paper.

Acknowledgements

We would like to thank Assist. Prof. Dr. Özge Karabıyık Acar for providing Cucurcitacin I.

Appendix A. Supporting information

Supplementary data associated with this article can be found in the online version at doi:10.1016/j.compbiolchem.2023.107934.

References

Aceto, N., Sausgruber, N., Brinkhaus, H., Gaidatzis, D., Martiny-Baron, G., Mazzarol, G., Confalonieri, S., Quarto, M., Hu, G., Balwierz, P.J., Pachkov, M., Elledge, S.J., van Nimwegen, E., Stadler, M.B., Bentires-Alj, M., 2012. Tyrosine phosphatase SHP2 promotes breast cancer progression and maintains tumor-initiating cells via activation of key transcription factors and a positive feedback signaling loop. Nat. Med 18, 529–537. https://doi.org/10.1038/nm.2645.

Akar, U., Ozpolat, B., Mehta, K., Lopez-Berestein, G., Zhang, D., Ueno, N.T., Hortobagyi, G.N., Arun, B., 2010. Targeting p70S6K prevented lung metastasis in a breast cancer xenograft model. Mol. Cancer Ther. 9, 1180–1187. https://doi.org/10.1158/1535-7163.MCT-09-1025.

Alafnan, A., Alamri, A., Hussain, T., Rizvi, S.M.D., 2022. Cucurbitacin-B exerts anticancer effects through instigation of apoptosis and cell cycle arrest within human prostate cancer PC3 cells via downregulating JAK/STAT signaling cascade. Pharmaceuticals 15. https://doi.org/10.3390/ph15101229.

Alzani, R., Pedrini, O., Albanese, C., Ceruti, R., Casolaro, A., Patton, V., Colotta, F., Rambaldi, A., Introna, M., Pesenti, E., Ciomei, M., Golay, J., 2010. Therapeutic efficacy of the pan-cdk inhibitor PHA-793887 in vitro and in vivo in engraftment and high-burden leukemia models. Exp. Hematol. 38 (259–269), e2 https://doi.org/10.1016/j.exphem.2010.02.004.

Arsic, N., Bendris, N., Peter, M., Begon-Pescia, C., Rebouissou, C., Gadéa, G., Bouquier, N., Bibeau, F., Lemmers, B., Blanchard, J.M., 2012. A novel function for Cyclin A2: Control of cell invasion via RhoA signaling. J. Cell Biol. 196, 147–162. https://doi.org/10.1083/jcb.201102085.

Ashburner, M., Ball, C.A., Blake, J.A., Botstein, D., Butler, H., Cherry, J.M., Davis, A.P., Dolinski, K., Dwight, S.S., Eppig, J.T., Harris, M.A., Hill, D.P., Issel-Tarver, L., Kasarskis, A., Lewis, S., Matese, J.C., Richardson, J.E., Ringwald, M., Rubin, G.M., Sherlock, G., 2000. Gene ontology: tool for the unification of biology. Nat. Genet. https://doi.org/10.1038/75556.

Bader, G.D., Hogue, C.W., 2003. An automated method for finding molecular complexes in large protein interaction networks.

Barrett, T., Wilhite, S.E., Ledoux, P., Evangelista, C., Kim, I.F., Tomashevsky, M., Marshall, K.A., Phillippy, K.H., Sherman, P.M., Holko, M., Yefanov, A., Lee, H., Zhang, N., Robertson, C.L., Serova, N., Davis, S., Soboleva, A., 2013. NCBI GEO: Archive for functional genomics data sets - update. Nucleic Acids Res 41, 991–995. https://doi.org/10.1093/nar/gks1193.

Baserga, R., Sell, C., Porcu, P., Rubini, M., Baserga, Renato, 1994. The role of the IGF-I receptor in the growth and transformation of mammalian cells. Cell ProliJ.

Bendris, N., Arsic, N., Lemmers, B., Blanchard, J.M., 2012. Cyclin A2, Rho GTPases and EMT. Small GTPases 3, 225–228. https://doi.org/10.4161/sgtp.20791.

Berman, A.Y., Manna, S., Schwartz, N.S., Katz, Y.E., Sun, Y., Behrmann, C.A., Yu, J.J., Plas, D.R., Alayev, A., Holz, M.K., 2017. ERRα regulates the growth of triple-negative breast cancer cells via S6K1-dependent mechanism. Signal Transduct. Target Ther. 2, 17035. https://doi.org/10.1038/sigtrans.2017.35.

Berman, H.M., Westbrook, J., Feng, Z., Gilliland, G., Bhat, T.N., Weissig, H., Shindyalov, I.N., Bourne, P.E., 2000. The protein data bank. Nucleic Acids Res.

Bi, Y., Kong, P., Zhang, L., Cui, H., Xu, X., Chang, F., Yan, T., Li, J., Cheng, C., Song, B., Niu, X., Liu, Xiangchen, Liu, Xue, Xu, E., Hu, X., Qian, Y., Wang, F., Li, H., Ma, Y., Yang, J., Liu, Y., Zhai, Y., Wang, Y., Zhang, Y., Liu, H., Liu, J., Wang, J., Cui, Y., Cheng, X., 2019. EP300 as an oncogene correlates with poor prognosis in esophageal squamous carcinoma. J. Cancer 10, 5413–5426. https://doi.org/10.7150/jca.34261.

Bolstad, B.M., Irizarry, R.A., Astrand, M., Speed, T.P., 2003. A comparison of normalization methods for high density oligonucleotide array data based on variance and bias. BIOINFORMATICS.

Brasca, M.G., Albanese, C., Alzani, R., Amici, R., Avanzi, N., Ballinari, D., Bischoff, J., Borghi, D., Casale, E., Croci, V., Fiorentini, F., Isacchi, A., Mercurio, C., Nesi, M., Orsini, P., Pastori, W., Pesenti, E., Pevarello, P., Roussel, P., Varasi, M., Volpi, D., Vulpetti, A., Ciomei, M., 2010a. Optimization of 6,6-dimethyl pyrrolo[3,4-c] pyrazoles: identification of PHA-793887, a potent CDK inhibitor suitable for intravenous dosing. Bioorg. Med. Chem. 18, 1844–1853. https://doi.org/10.1016/j.bmc.2010.01.042.

Brasca, M.G., Albanese, C., Alzani, R., Amici, R., Avanzi, N., Ballinari, D., Bischoff, J., Borghi, D., Casale, E., Croci, V., Fiorentini, F., Isacchi, A., Mercurio, C., Nesi, M., Orsini, P., Pastori, W., Pesenti, E., Pevarello, P., Roussel, P., Varasi, M., Volpi, D., Vulpetti, A., Ciomei, M., 2010b. Optimization of 6,6-dimethyl pyrrolo[3,4-c] pyrazoles: identification of PHA-793887, a potent CDK inhibitor suitable for intravenous dosing. Bioorg. Med. Chem. 18, 1844–1853. https://doi.org/10.1016/j.bmc.2010.01.042.

Brockes, J.P., Kumar, A., 2008. Comparative aspects of animal regeneration. Annu Rev. Cell Dev. Biol. https://doi.org/10.1146/annurev.cellbio.24.110707.175336.
Cao, Y., Duan, H., Su, A., Xu, L., Lai, B., 2022. A pan-cancer analysis confirms PTPN11's potential as a prognostic and immunological biomarker. Aging (Albany NY) 14, 5590–5610.
Carbon, S., Douglass, E., Good, B.M., Unni, D.R., Harris, N.L., Mungall, C.J., Basu, S., Chisholm, R.L., Dodson, R.J., Hartline, E., Fey, P., Thomas, P.D., Albou, L.P., Ebert, D., Kesling, M.J., Mi, H., Muruganujan, A., Huang, X., Mushayahama, T., LaBonte, S.A., Siegele, D.A., Antonazzo, G., Attrill, H., Brown, N.H., Garapati, P., Marygold, S.J., Trovisco, V., dos Santos, G., Falls, K., Tabone, C., Zhou, P., Goodman, J.L., Strelets, V.B., Thurmond, J., Garmiri, P., Ishtiaq, R., Rodríguez-López, M., Acencio, M.L., Kuiper, M., Lægreid, A., Logie, C., Lovering, R.C., Kramarz, B., Saverimuttu, S.C.C., Pinheiro, S.M., Gunn, H., Su, R., Thurlow, K.E., Chibucos, M., Giglio, M., Nadendla, S., Munro, J., Jackson, R., Duesbury, M.J., Del-Toro, N., Meldal, B.H.M., Paneerselvam, K., Perfetto, L., Porras, P., Orchard, S., Shrivastava, A., Chang, H.Y., Finn, R.D., Mitchell, A.L., Rawlings, N.D., Richardson, L., Sangrador-Vegas, A., Blake, J.A., Christie, K.R., Dolan, M.E., Drabkin, H.J., Hill, D.P., Ni, L., Sitnikov, D.M., Harris, M.A., Oliver, S.G., Rutherford, K., Wood, V., Hayles, J., Bähler, J., Bolton, E.R., de Pons, J.L., Dwinell, M.R., Hayman, G.T., Kaldunski, M.L., Kwitek, A.E., Lauledekind, S.J.F., Plasterer, C., Tutaj, M.A., Vedi, M., Wang, S.J., D'Eustachio, P., Matthews, L., Balhoff, J.P., Aleksander, S.A., Alexander, M.J., Cherry, J.M., Engel, S.R., Gondwe, F., Karra, K., Miyasato, S.R., Nash, R.S., Simison, M., Skrzypek, M.S., Weng, S., Wong, E.D., Feuermann, M., Gaudet, P., Morgat, A., Bakker, E., Berardini, T.Z., Reiser, L., Subramaniam, S., Huala, E., Arighi, C.N., Auchincloss, A., Axelsen, K., Argoud-Puy, G., Bateman, A., Blatter, M.C., Boutet, E., Bowler, E., Breuza, L., Bridge, A., Britto, R., Bye-A-Jee, H., Casas, C.C., Coudert, E., Denny, P., Es-Treicher, A., Famiglietti, M.L., Georghiou, G., Gos, A.N., Gruaz-Gumowski, N., Hatton-Ellis, E., Hulo, C., Ignatchenko, A., Jungo, F., Laiho, K., le Mercier, P., Lieberherr, D., Lock, A., Lussi, Y., MacDougall, A., Ma-Grane, M., Martin, M.J., Masson, P., Natale, D.A., Hyka-Nouspikel, N., Orchard, S., Pedruzzi, I., Pourcel, L., Poux, S., Pundir, S., Rivoire, C., Speretta, E., Sundaram, S., Tyagi, N., Warner, K., Zaru, R., Wu, C.H., Diehl, A.D., Chan, J.N., Grove, C., Lee, R.Y.N., Muller, H.M., Raciti, D., van Auken, K., Sternberg, P.W., Berriman, M., Paulini, M., Howe, K., Gao, S., Wright, A., Stein, L., Howe, D.G., Toro, S., Westerfield, M., Jaiswal, P., Cooper, L., Elser, J., 2021. The gene ontology resource: enriching a GOld mine. Nucleic Acids Res. 49, D325–D334. https://doi.org/10.1093/nar/gkaa1113.
Carboni, J.M., Wittman, M., Yang, Z., Lee, F., Greer, A., Hurlburt, W., Hillerman, S., Cao, C., Cantor, G.H., Dell-John, J., Chen, C., Discenza, L., Menard, K., Li, A., Trainor, G., Vyas, D., Kramer, R., Attar, R.M., Gottardis, M.M., 2009. BMS-754807, a small molecule inhibitor of insulin-like growth factor-1R/IR. Mol. Cancer Ther. 8, 3341–3349. https://doi.org/10.1158/1535-7163.MCT-09-0499.
Carboni, Joan M., Wittman, M., Yang, Z., Lee, F., Greer, A., Hurlburt, W., Hillerman, S., Cao, C., Cantor, G.H., Dell-John, J., Chen, C., Discenza, L., Menard, K., Li, A., Trainor, G., Vyas, D., Kramer, R., Attar, R.M., Gottardis, M.M., 2009. BMS-754807, a small molecule inhibitor of insulin-like growth factor-1R/IR. Mol. Cancer Ther. 8, 3341–3349. https://doi.org/10.1158/1535-7163.MCT-09-0499.
Chamankhah, M., Eftekharpour, E., Karimi-abdolrezaee, S., Boutros, P.C., San-marina, S., Fehlings, M.G., 2013. Genome-wide gene expression profiling of stress response in a spinal cord clip compression injury model.
Chan, R.J., Feng, G.-S., 2007. PTPN11 is the first identified proto-oncogene that encodes a tyrosine phosphatase. Blood. https://doi.org/10.1182/blood.
Chau, M.N., Banerjee, P.P., 2008. Development of a STAT3 reporter prostate cancer cell line for high throughput screening of STAT3 activators and inhibitors. Biochem Biophys. Res. Commun. 377, 627–631. https://doi.org/10.1016/J.BBRC.2008.10.025.
Chen, Z., Chen, C., Li, L., Zhang, T., Wang, X., 2021. Pan-cancer analysis reveals That E1A binding protein p300 mutations increase genome instability and antitumor immunity. Front Cell Dev. Biol. 9. https://doi.org/10.3389/fcell.2021.729927.
Clark, N.R., Hu, K.S., Feldmann, A.S., Kou, Y., Chen, E.Y., Duan, Q., Ma'ayan, A., 2014. The characteristic direction: a geometrical approach to identify differentially expressed genes. BMC Bioinforma. 15, 79. https://doi.org/10.1186/1471-2105-15-79.
Dandawate, P., Subramaniam, D., Panovich, P., Standing, D., Krishnamachary, B., Kaushik, G., Thomas, S.M., Dhar, A., Weir, S.J., Jensen, R.A., Anant, S., 2020. Cucurbitacin B and I inhibits colon cancer growth by targeting the Notch signaling pathway. Sci. Rep. 10. https://doi.org/10.1038/s41598-020-57940-9.
Dayyani, F., Parikh, N.U., Varkaris, A.S., Song, J.H., Moorthy, S., Chatterji, T., Maity, S. N., Wolfe, A.R., Carboni, J.M., Gottardis, M.M., Logothetis, C.J., Gallick, G.E., 2012. Combined inhibition of IGF-1R/IR and Src family kinases enhances antitumor effects in prostate cancer by decreasing activated survival pathways. PLoS One 7. https://doi.org/10.1371/journal.pone.0051189.
Demircan, T., 2020. Dissecting the molecular signature of spinal cord regeneration in the axolotl model. Cureus 12. https://doi.org/10.7759/cureus.7014.
Demirci, Y., Heger, G., Katkat, E., Papatheodorou, I., Brazma, A., Ozhan, G., 2022. Brain regeneration resembles brain cancer at its early wound healing stage and diverges from cancer later at its proliferation and differentiation stages. Front Cell Dev. Biol. 10. https://doi.org/10.3389/fcell.2022.813314.
Diaz Quiroz, J.F., Tsai, E., Coyle, M., Sehm, T., Echeverri, K., 2014. Precise control of miR-125b levels is required to create a regeneration-permissive environment after spinal cord injury: a cross-species comparison between salamander and rat. DMM Dis. Models Mech. 7, 601–611. https://doi.org/10.1242/dmm.014837.
Duan, Q., Reid, S.P., Clark, N.R., Wang, Z., Fernandez, N.F., Rouillard, A.D., Readhead, B., Tritsch, S.R., Hodos, R., Hafner, M., Niepel, M., Sorger, P.K., Dudley, J. T., Bavari, S., Panchal, R.G., Ma'ayan, A., 2016. L1000CDS2: LINCS L1000 characteristic direction signatures search engine. NPJ Syst. Biol. Appl. 2, 16015. https://doi.org/10.1038/npjsba.2016.15.
Duncan, K.L.K., Duncan, M.D., Alley, M.C., Sausville, E.A., 1996. Cucurbitacin E-induced disruption of the actin and vimentin cytoskeleton in prostate carcinoma cells. Biochem Pharm. 52, 1553–1560. https://doi.org/10.1016/S0006-2952(96)00557-6.
Dwaraka, V.B., Smith, J.J., Woodcock, M.R., Voss, S.R., 2019. Comparative transcriptomics of limb regeneration: Identification of conserved expression changes among three species of Ambystoma. Genomics 111, 1216–1225. https://doi.org/10.1016/j.ygeno.2018.07.017.
Eberhardt, J., Santos-Martins, D., Tillack, A.F., Forli, S., 2021. AutoDock Vina 1.2.0: new docking methods, expanded force field, and Python bindings. J. Chem. Inf. Model.
Eckner, R., Ewen, M.E., Newsome, D., Gerdes, M., Decaprio, J.A., Lawrence, J.B., Livingston, D.M., 1994. Molecular cloning and functional analysis of the adenovirus E1A-assoclated 300-kD protein.(p300) reveals a protein with properties oI a transcriptional adaptor.
Fabregat, A., Sidiropoulos, K., Garapati, P., Gillespie, M., Hausmann, K., Haw, R., Jassal, B., Jupe, S., Korninger, F., McKay, S., Matthews, L., May, B., Milacic, M., Rothfels, K., Shamovsky, V., Webber, M., Weiser, J., Williams, M., Wu, G., Stein, L., Hermjakob, H., D'Eustachio, P., 2016. The Reactome pathway Knowledgebase. Nucleic Acids Res 44, D481–D487. https://doi.org/10.1093/nar/gkv1351.
Feitsma, H., Cuppen, E., 2008. Zebrafish as a cancer model. Mol. Cancer Res. https://doi.org/10.1158/1541-7786.MCR-07-2167.
Fumagalli, M.R., Zapperi, S., la Porta, C.A.M., 2018. Regeneration in distantly related species: common strategies and pathways. NPJ Syst. Biol. Appl. 4. https://doi.org/10.1038/s41540-017-0042-z.
Gan, Y., Li, Y., Li, T., Shu, G., Yin, G., 2018. CCNA2 acts as a novel biomarker in regulating the growth and apoptosis of colorectal cancer. Cancer Manag Res 10, 5113–5124. https://doi.org/10.2147/CMAR.S176833.
Gao, T., Han, Y., Yu, L., Ao, S., Li, Z., Ji, A., 2014. CCNA2 is a prognostic biomarker for ER+ breast cancer and tamoxifen resistance. PLoS One 9. https://doi.org/10.1371/journal.pone.0091771.
Gao, Y., Islam, M.S., Tian, J., Lui, V.W.Y., Xiao, D., 2014. Inactivation of ATP citrate lyase by cucurbitacin B: a bioactive compound from cucumber, inhibits prostate cancer growth. Cancer Lett. 349, 15–25. https://doi.org/10.1016/j.canlet.2014.03.015.
Gautier, L., Cope, L., Bolstad, B.M., Irizarry, R.A., 2004. Affy - analysis of affymetrix GeneChip data at the probe level. Bioinformatics 20, 307–315. https://doi.org/10.1093/bioinformatics/btg405.
Gayther, S.A., Batley, S.J., Linger, L., Bannister, A., Thorpe, K., Chin, S.-F., Daigo, Y., Russell, P., Wilson, A., Sowter, H.M., Delhanty, J.D.A., Ponder, B.A.J., Kouzarides, T., Caldas, C., 2000. Mutations truncating the EP300 acetylase in human cancers. Nat. Genet 24, 300–303. https://doi.org/10.1038/73536.
Gentleman, R.C., Carey, V.J., Bates, D.M., Bolstad, B., Dettling, M., Dudoit, S., Ellis, B., Gautier, L., Ge, Y., Gentry, J., Hornik, K., Hothorn, T., Huber, W., Iacus, S., Irizarry, R., Leisch, F., Li, C., Maechler, M., Rossini, A.J., Sawitzki, G., Smith, C., Smyth, G., Tierney, L., Yang, J.Y., Zhang, J., 2004. Open access bioconductor: open software development for computational biology and bioinformatics. Genome Biol.
Gurung, A.B., Bhattacharjee, A., Ali, M.A., 2016. Exploring the physicochemical profile and the binding patterns of selected novel anticancer Himalayan plant derived active compounds with macromolecular targets. Inf. Med. Unlocked 5, 1–14. https://doi.org/10.1016/j.imu.2016.09.004.
Halvorson, K.G., Barton, K.L., Schroeder, K., Misuraca, K.L., Hoeman, C., Chung, A., Crabtree, D.M., Cordero, F.J., Singh, R., Spasojevic, I., Berlow, N., Pal, R., Becher, O. J., 2015. A high-throughput in Vitro drug screen in a genetically engineered mouse model of diffuse intrinsic pontine glioma identifies BMS-754807 as a promising therapeutic agent. PLoS One 10, 1–16. https://doi.org/10.1371/journal.pone.0118926.
He, X., Gao, Q., Qiang, Y., Guo, W., Ma, Y., 2017. Cucurbitacin E induces apoptosis of human prostate cancer cells via cofilin-1 and mTORC1. Oncol. Lett. 13, 4905–4910. https://doi.org/10.3892/ol.2017.6086.
Hill, K.S., Roberts, E.R., Wang, X., Marin, E., Park, T.D., Son, S., Ren, Y., Fang, B., Yoder, S., Kim, S., Wan, L., Sarnaik, A.A., Koomen, J.M., Messina, J.L., Teer, J.K., Kim, Y., Wu, J., Chalfant, C.E., Kim, M., 2019. PTPN11 plays oncogenic roles and is a therapeutic target for BRAF wild-type melanomas. Mol. Cancer Res. 17, 583–593. https://doi.org/10.1158/1541-7786.MCR-18-0777.
Huang, Y.-H., Cai, K., Xu, P.-P., Wang, L., Huang, C.-X., Fang, Y., Cheng, S., Sun, X.-J., Liu, F., Huang, J.-Y., Ji, M.-M., Zhao, W.-L., 2021. CREBBP/EP300 mutations promoted tumor progression in diffuse large B-cell lymphoma through altering tumor-associated macrophage polarization via FBXW7-NOTCH-CCL2/CSF1 axis. Signal Transduct. Target Ther. 6, 10. https://doi.org/10.1038/s41392-020-00437-8.
Hui, S.P., Sengupta, D., Gek, S., Lee, P., Sen, T., Kundu, S., 2014. Genome wide expression profiling during spinal cord regeneration identifies comprehensive cellular responses in zebrafish. PLoS One 9. https://doi.org/10.1371/journal.pone.0084212.
Jabir, N.R., Rehman, M.T., Alsolami, K., Shakil, S., Zughaibi, T.A., Alserihi, R.F., Khan, M.S., AlAjmi, M.F., Tabrez, S., 2021. Concatenation of molecular docking and molecular simulation of BACE-1, γ-secretase targeted ligands: in pursuit of Alzheimer's treatment. Ann. Med 53, 2332–2344. https://doi.org/10.1080/07853890.2021.2009124.
Janaki Ramaiah, M., Lavanya, A., Honarpisheh, M., Zarea, M., Bhadra, U., Bhadra, M.P., 2014. miR-15/16 complex targets p70S6 kinase1 and controls cell proliferation in MDA-MB-231 breast cancer cells. Gene 552, 255–264. https://doi.org/10.1016/j.gene.2014.09.052.
Jimeno, R., Mouron, S., Salgado, R., Loi, S., Pérez-Mies, B., Sánchez-Bayona, R., Manso, L., Martínez, M., Garrido-García, A., Serrano-Pardo, R., Colomer, R., Quintela-Fandino, M., 2022. Tumor P70S6K hyperactivation is inversely associated

with tumor-infiltrating lymphocytes in triple-negative breast cancer. Clin. Transl. Oncol. https://doi.org/10.1007/s12094-022-03006-3.
Kanehisa, M., Araki, M., Goto, S., Hattori, M., Hirakawa, M., Itoh, M., Katayama, T., Kawashima, S., Okuda, S., Tokimatsu, T., Yamanishi, Y., 2008. KEGG for linking genomes to life and the environment. Nucleic Acids Res. 36, D480–D484. https://doi.org/10.1093/nar/gkm882.
Kim, S., Chen, J., Cheng, T., Gindulyte, A., He, J., He, S., Li, Q., Shoemaker, B.A., Thiessen, P.A., Yu, B., Zaslavsky, L., Zhang, J., Bolton, E.E., 2019. PubChem 2019 update: improved access to chemical data. Nucleic Acids Res 47, D1102–D1109. https://doi.org/10.1093/nar/gky1033.
Ko, E., Kim, Y., Cho, E.Y., Han, J., Shim, Y.M., Park, J., Kim, D.-H., 2013. Synergistic effect of Bcl-2 and Cyclin A2 on adverse recurrence-free survival in stage I non-small cell lung cancer. Ann. Surg. Oncol. 20, 1005–1012. https://doi.org/10.1245/s10434-012-2727-2.
Kolb, E.A., Gorlick, R., Lock, R., Carol, H., Morton, C.L., Keir, S.T., Reynolds, C.P., Min, H., Maris, J.M., Billups, C., Smith, M.A., Houghton, P.J., 2014. NIH Public Access 56, 595–603. https://doi.org/10.1002/pbc.22741.Initial.
Kolde, R., 2012. Pheatmap: pretty heatmaps. R. Package Version 1, 726.
Kubat Oktem, E., Aydin, B., Yazar, M., Arga, K.Y., 2022. Integrative analysis of motor neuron and microglial transcriptomes from SOD1G93A mice models uncover potential drug treatments for ALS. J. Mol. Neurosci. https://doi.org/10.1007/s12031-022-02071-1.
Lee, L.M.J., Seftor, E.A., Bonde, G., Cornell, R.A., Hendrix, M.J.C., 2005. The fate of human malignant melanoma cells transplanted into zebrafish embryos: assessment of migration and cell division in the absence of tumor formation. Dev. Dyn. 233, 1560–1570. https://doi.org/10.1002/dvdy.20471.
Li, R., Xiao, J., Tang, S., Lin, X., Xu, H., Han, B., Yang, M., Liu, F., 2020. Cucurbitacin I induces apoptosis in ovarian cancer cells through oxidative stress and the p190B-Rac1 signaling axis. Mol. Med. Rep. 22, 2545–2550. https://doi.org/10.3892/mmr.2020.11327.
Li, Y., Chen, M., Chen, Q., Yuan, M., Zeng, X., Zeng, Y., He, M., Wang, B., Han, B., 2023. Bioinformatics identification of therapeutic gene targets for gastric cancer. Adv. Ther. 40, 1456–1473. https://doi.org/10.1007/s12325-023-02428-x.
Malumbres, M., Barbacid, M., 2009. Cell cycle, CDKs and cancer: a changing paradigm. Nat. Rev. Cancer. https://doi.org/10.1038/nrc2602.
Massard, C., Soria, J.C., Anthoney, D.A., Proctor, A., Scaburri, A., Pacciarini, M.A., Laffranchi, B., Pellizzoni, C., Kroemer, G., Armand, J.P., Balheda, R., Twelves, C.J., 2011. A first in man, phase I dose-escalation study of PHA-793887, an inhibitor of multiple cyclin-dependent kinases (CDK2, 1 and 4) reveals unexpected hepatotoxicity in patients with solid tumors. Cell Cycle 10, 963–970. https://doi.org/10.4161/cc.10.6.15075.
Miyamoto, D., Miyamoto, M., Takahashi, A., Yomogita, Y., Higashi, H., Kondo, S., Hatakeyama, M., 2008. Isolation of a distinct class of gain-of-function SHP-2 mutants with oncogenic RAS-like transforming activity from solid tumors. Oncogene 27, 3508–3515. https://doi.org/10.1038/sj.onc.1211019.
Molecule, I.S., Fuentes-baile, M., Ventero, P., Encinar, J.A., Garc, P., 2020. cancers.
Monaghan, J.R., Walker, J.A., Page, R.B., Putta, S., Beachy, C.K., Voss, S.R., 2007. Early gene expression during natural spinal cord regeneration in the salamander Ambystoma mexicanum. J. Neurochem. 101, 27–40. https://doi.org/10.1111/j.1471-4159.2006.04344.x.
Montecucco, A., Zanetta, F., Biamonti, G., 2015. Molecular mechanisms of etoposide. EXCLI J. https://doi.org/10.17179/excli2014-561.
Morris, G.M., Ruth, H., Lindstrom, W., Sanner, M.F., Belew, R.K., Goodsell, D.S., Olson, A.J., 2009. Software news and updates AutoDock4 and AutoDockTools4: automated docking with selective receptor flexibility. J. Comput. Chem. 30, 2785–2791. https://doi.org/10.1002/jcc.21256.
Nguyen, B.C.Q., Taira, N., Maruta, H., Tawata, S., 2016. Artepillin C and other herbal PAK1-Blockers: effects on hair cell proliferation and related PAK1-dependent biological function in cell culture. Phytother. Res. 30, 120–127. https://doi.org/10.1002/ptr.5510.
Ni, Y., Wu, S., Wang, X., Zhu, G., Chen, X., Ding, Y., Jiang, W., 2018. Cucurbitacin I induces pro-death autophagy in A549 cells via the ERK-mTOR-STAT3 signaling pathway. J. Cell Biochem. 119, 6104–6112. https://doi.org/10.1002/jcb.26808.
Oktem, E.K., Yazar, M., 2022. Drug repositioning identifies six drug candidates for systemic autoimmune diseases by integrative analyses of transcriptomes from scleroderma, systemic lupus erythematosus, and Sjogren's syndrome. OMICS. https://doi.org/10.1089/omi.2022.0138.
Öktem, E.K., Yazar, M., Gulfidan, G., Arga, K.Y., 2019. Cancer drug repositioning by comparison of gene expression in humans and axolotl (Ambystoma mexicanum) during wound healing. OMICS 23, 389–405. https://doi.org/10.1089/omi.2019.0093.
Oughtred, R., Stark, C., Breitkreutz, B.-J., Rust, J., Boucher, L., Chang, C., Kolas, N., O'Donnell, L., Leung, G., McAdam, R., 2019. The BioGRID interaction database: 2019 update. Nucleic Acids Res 47, D529–D541.
Oviedo, N.J., Beane, W.S., 2009. Regeneration: the origin of cancer or a possible cure. Semin Cell Dev. Biol. https://doi.org/10.1016/j.semcdb.2009.04.005.
Pérez-Tenorio, G., Stål, O., Group, and members of the S.S.B.C, 2002. Activation of AKT/PKB in breast cancer predicts a worse outcome among endocrine treated patients. Br. J. Cancer 86, 540–545. https://doi.org/10.1038/sj.bjc.6600126.
Pollak, M.N., Schernhammer, E.S., Hankinson, S.E., 2004. Insulin-like growth factors and neoplasia. Nat. Rev. Cancer. https://doi.org/10.1038/nrc1387.
Qin, S., Gao, H., Kim, W., Zhang, H., Gu, Y., Kalari, K.R., Sinnwell, J.P., Scholz, J.A., Xie, F., Yin, P., Yu, J., Qin, B., Zhuang, Y., Wei, L., Tan, W., Bryce, A.H., Weinshilboum, R.M., Wang, L., 2022. Biomarkers for predicting abiraterone treatment outcome and selecting alternative therapies in castration-resistant prostate cancer. Clin. Pharm. Ther. 111, 1296–1306. https://doi.org/10.1002/cpt.2582.
Razaviyan, J., Hadavi, R., Tavakoli, R., Kamani, F., Paknejad, M., Mohammadi-Yeganeh, S., 2018. Expression of miRNAs targeting mTOR and S6K1 genes of mTOR signaling pathway including miR-96, miR-557, and miR-3182 in triple-negative breast cancer. Appl. Biochem. Biotechnol. 186, 1074–1089. https://doi.org/10.1007/s12010-018-2773-8.
Ricci, L., Srivastava, M., 2018. Wound-induced cell proliferation during animal regeneration. Wiley Inter. Rev. Dev. Biol. https://doi.org/10.1002/wdev.321.
Sabin, K., Santos-ferreira, T., Essig, J., Rudasill, S., Echeverri, K., 2015. Dynamic membrane depolarization is an early regulator of ependymoglial cell response to spinal cord injury in axolotl. Dev. Biol. 408, 14–25. https://doi.org/10.1016/j.ydbio.2015.10.012.
Sachdev, D., Yee, D., 2007. Disrupting insulin-like growth factor signaling as a potential cancer therapy. Mol. Cancer Ther. https://doi.org/10.1158/1535-7163.MCT-06-0080.
Sean, D., Meltzer, P.S., 2007. GEOquery: a bridge between the gene expression omnibus (GEO) and BioConductor. Bioinformatics 23, 1846–1847. https://doi.org/10.1093/bioinformatics/btm254.
Shannon, P., Markiel, A., Ozier, O., Baliga, N.S., Wang, J.T., Ramage, D., Amin, N., Schwikowski, B., Ideker, T., 2003. Cytoscape: a software environment for integrated models of biomolecular interaction networks. Genome Res 13, 2498–2504. https://doi.org/10.1101/gr.1239303.
Shen, J., Li, L., Yang, T., Cheng, N., Sun, G., 2019. Drug sensitivity screening and targeted pathway analysis reveal a multi-driver proliferative mechanism and suggest a strategy of combination targeted therapy for colorectal cancer cells. Molecules 24. https://doi.org/10.3390/molecules24030623.
Sikander, M., Malik, S., Chauhan, N., Khan, P., Kumari, S., Kashyap, V.K., Khan, S., Ganju, A., Halaweish, F.T., Yallapu, M.M., Jaggi, M., Chauhan, S.C., 2019. Cucurbitacin D reprograms glucose metabolic network in prostate cancer. Cancers 11, 1–17. https://doi.org/10.3390/cancers11030364 (Basel).
Smedley, D., Haider, S., Durinck, S., Pandini, L., Provero, P., Allen, J., Arnaiz, O., Awedh, M.H., Baldock, R., Barbiera, G., Bardou, P., Beck, T., Blake, A., Bonierbale, M., Brookes, A.J., Bucci, G., Buetti, I., Burge, S., Cabau, C., Carlson, J.W., Chelala, C., Chrysostomou, C., Cittaro, D., Collin, O., Cordova, R., Cutts, R.J., Dassi, E., di Genova, A., Djari, A., Esposito, A., Estrella, H., Eyras, E., Fernandez-Banet, J., Forbes, S., Free, R.C., Fujisawa, T., Gadaleta, E., Garcia-Manteiga, J.M., Goodstein, D., Gray, K., Guerra-Assunção, J.A., Haggarty, B., Han, D.J., Han, B.W., Harris, T., Harshbarger, J., Hastings, R.K., Hayes, R.D., Hoede, C., Hu, S., Hu, Z.L., Hutchins, L., Kan, Z., Kawaji, H., Keliet, A., Kerhornou, A., Kim, S., Kinsella, R., Klopp, C., Kong, L., Lawson, D., Lazarevic, D., Lee, J.H., Letellier, T., Li, C.Y., Lio, P., Liu, C.J., Luo, J., Maass, A., Mariette, J., Maurel, T., Merella, S., Mohamed, A.M., Moreews, F., Nabihoudine, I., Ndegwa, N., Noirot, C., Perez-Llamas, C., Primig, M., Quattrone, A., Quesneville, H., Rambaldi, D., Reecy, J., Riba, M., Rosanoff, S., Saddiq, A.A., Salas, E., Sallou, O., Shepherd, R., Simon, R., Sperling, L., Spooner, W., Staines, D.M., Steinbach, D., Stone, K., Stupka, E., Teague, J.W., Dayem Ullah, A.Z., Wang, J., Ware, D., Wong-Erasmus, M., Youens-Clark, K., Zadissa, A., Zhang, S.J., Kasprzyk, A., 2015. The BioMart community portal: an innovative alternative to large, centralized data repositories. Nucleic Acids Res 43, W589–W598. https://doi.org/10.1093/nar/gkv350.
Smyth, G.K., 2004. Linear models and empirical bayes methods for assessing differential expression in microarray experiments. Stat. Appl. Genet. Mol. Biol. 3. https://doi.org/10.2202/1544-6115.1027.
Smyth, G.K., Ritchie, M., Thorne, N., Wettenhall, J., 2005. LIMMA: linear models for microarray data. Bioinformatics and Computational Biology Solutions Using R and Bioconductor. Statistics for Biology and Health.
Sohn, J., Do, K.A., Liu, S., Chen, H., Mills, G.B., Hortobagyi, G.N., Meric-Bernstam, F., Gonzalez-Angulo, A.M., 2013. Functional proteomics characterization of residual triple-negative breast cancer after standard neoadjuvant chemotherapy. Ann. Oncol. 24, 2522–2526. https://doi.org/10.1093/annonc/mdt248.
Sundaram, G.M., Quah, S., Sampath, P., 2018. Cancer: the dark side of wound healing. FEBS J. https://doi.org/10.1111/febs.14586.
Szklarczyk, D., Santos, A., von Mering, C., Jensen, L.J., Bork, P., Kuhn, M., 2016. STITCH 5: augmenting protein-chemical interaction networks with tissue and affinity data. Nucleic Acids Res 44, D380–D384. https://doi.org/10.1093/nar/gkv1277.
Tian, W., Chen, C., Lei, X., Zhao, J., Liang, J., 2018. CASTp 3.0: computed atlas of surface topography of proteins. Nucleic Acids Res 46, W363–W367. https://doi.org/10.1093/nar/gky473.
Tica, J., Didangelos, A., 2018. Comparative transcriptomics of rat and axolotl after spinal cord injury dissects differences and similarities in inflammatory and matrix remodeling gene expression patterns. Front Neurosci. 12. https://doi.org/10.3389/fnins.2018.00808.
Uhlen, M., Oksvold, P., Fagerberg, L., Lundberg, E., Jonasson, K., Forsberg, M., Zwahlen, M., Kampf, C., Wester, K., Hober, S., Wernerus, H., Björling, L., Ponten, F., 2010. Towards a knowledge-based human protein atlas. Nat. Biotechnol. 28, 1248–1250. https://doi.org/10.1038/nbt1210-1248.
Villa, E., Ali, E.S., Sahu, U., Ben-Sahra, I., 2019. Cancer cells tune the signaling pathways to empower de novo synthesis of nucleotides. Cancers (Basel). https://doi.org/10.3390/cancers11050688.
Wang, L., Ji, X.B., Wang, L.H., Xia, Z.K., Xie, Y.X., Liu, W.J., Qiu, J.G., Jiang, B.H., Liu, L.Z., 2021. MiRNA-30e downregulation increases cancer cell proliferation, invasion and tumor growth through targeting RPS6KB1. Aging (Albany NY) 13, 24037–24049.
Wishart, D.S., Feunang, Y.D., Guo, A.C., Lo, E.J., Marcu, A., Grant, J.R., Sajed, T., Johnson, D., Li, C., Sayeeda, Z., Assempour, N., Iynkkaran, I., Liu, Y., MacIejewski, A., Gale, N., Wilson, A., Chin, L., Cummings, R., Le, Di, Pon, A., Knox, C., Wilson, M., 2018. DrugBank 5.0: a major update to the DrugBank database

for 2018. Nucleic Acids Res. 46, D1074–D1082. https://doi.org/10.1093/nar/gkx1037.

Wu, B., Yang, W., Fu, Z., Xie, H., Guo, Z., Liu, D., Ge, J., Zhong, S., Liu, L., Liu, J., Zhu, D., 2021. Selected using bioinformatics and molecular docking analyses, PHA-793887 is effective against osteosarcoma. Aging 13, 16425–16444. https://doi.org/10.18632/aging.203165.

Yang, Q., Qiu, H., Xie, H., Qi, Y., Cha, H., Qu, J., Wang, M., Feng, Y., Ye, X., Mu, J., Huang, J., 2017. A schistosoma japonicum infection promotes the expansion of myeloid-derived suppressor cells by activating the JAK/STAT3 pathway. J. Immunol. 198, 4716–4727. https://doi.org/10.4049/jimmunol.1601860.

Yang, W., Wang, J., Moore, D.C., Liang, H., Dooner, M., Wu, Q., Terek, R., Chen, Q., Ehrlich, M.G., Quesenberry, P.J., Neel, B.G., 2013. Ptpn11 deletion in a novel progenitor causes metachondromatosis by inducing hedgehog signalling. Nature 499, 491–495. https://doi.org/10.1038/nature12396.

Zhang, J., Zhang, F., Niu, R., 2015. Functions of Shp2 in cancer. J. Cell Mol. Med. 19, 2075–2083. https://doi.org/10.1111/jcmm.12618.

Zhou, Y., Zhou, B., Pache, L., Chang, M., Khodabakhshi, A.H., Tanaseichuk, O., Benner, C., Chanda, S.K., 2019. Metascape provides a biologist-oriented resource for the analysis of systems-level datasets. Nat. Commun. 10, 1523. https://doi.org/10.1038/s41467-019-09234-6.